Ocean Engineering 303 (2024) 117802

Contents lists available at ScienceDirect

Ocean Engineering

journal homepage: www.elsevier.com/locate/oceaneng

Importance of the soil–structure interaction in the optimisation of the jacket designs of offshore wind turbines

Román Quevedo-Reina [a], Guillermo M. Álamo [a,*], Stijn François [b], Geert Lombaert [b], Juan J. Aznárez [a]

[a] Instituto Universitario de Sistemas Inteligentes y Aplicaciones Numéricas en Ingeniería, Universidad de Las Palmas de Gran Canaria, Edif. Central del Parque Científico-Tecnológico. Campus Universitario de Tafira, Las Palmas de Gran Canaria, 35017, Spain
[b] Department of Civil Engineering, KU Leuven, Kasteelpark Arenberg 40, Leuven, 3001, Belgium

ARTICLE INFO

Keywords:
Offshore wind turbine
Soil–structure interaction effects
Jacket structure
Pile foundation
Structural optimisation

ABSTRACT

Advances in the design process and understanding of the structural behaviour of jacket-type foundations for offshore wind turbines are fundamental to the expansion of these devices in medium-depth waters. The structural evaluation of jacket foundations is a complex and computationally expensive task because of the large number of structural elements and numerous load scenarios and requirements imposed by international standards. In this context, the soil–structure interaction is not usually incorporated into the optimisation process of these devices, assuming that the foundation flexibility does not significantly affect the supporting structure. This study investigated an approach for analysing the influence of the soil–structure interaction on the structural design. To perform a relevant analysis, an optimisation process was used to obtain feasible designs for a 10-MW wind turbine in a specific location. To optimise and evaluate the jackets, a structural model based on static equivalent analysis of the most representative load scenarios for environmental loads was used. The obtained designs highlight the importance of considering the soil–structure interaction for evaluating the technical requirements imposed on these structures, especially in the ultimate limit states.

1. Introduction

Wind power technology has experienced significant growth in recent years, and an increasing prevalence of offshore wind farms has been observed owing to better offshore wind conditions and fewer space limitations for their installation (Wang et al., 2022). According to the Offshore Wind Market Report, which analysed more than 200 global operating offshore wind energy projects up to 2020 (Musial et al., 2021), monopile foundations are the most frequent choice for these devices, representing 74.8% of the total, followed by jacket substructures at 10.8%. However, this trend is different for announced projects (Musial et al., 2021), where monopiles and jackets account for 51.6% and 21.5%, respectively. This change is mainly due to the increase in manufacturing options and depths at which wind turbines are installed.

The correct design of jacket structures that support offshore wind turbines (OWTs) is very important for the expansion of this technology and, therefore, for the achievement of renewable energy objectives. However, this calculation is complex because it requires the evaluation of numerous load cases and the verification of many structural elements. Some authors have developed optimisation procedures to obtain efficient jacket designs. Oest et al. (2017) optimised a jacket based on a previous design using sequential linear programming. Chew et al. (2016) optimised a jacket structure using a sequential quadratic programming approach. Stolpe et al. (2017) addressed the optimisation of a jacket structure as a support for a larger wind turbine (10 MW) through a mixed optimisation strategy that defined the main topological aspects of the structure using pattern search optimisation, while sizing the sections using gradient-based methods. In addition, using sequential linear programming, Couceiro et al. (2020) optimised a jacket by considering different levels of bracing and compared the results. Ju and Hsieh (2022) used Powell's method to optimise the jacket support structure of 10-MW and 15-MW wind turbines with three and four legs at water depths of 35, 50, and 80 m and performed a preliminary analysis of the influence of these variables on the total mass of the foundation. All the above studies used structural simulations in the time domain, except for Oest et al. (2017), who performed a static analysis for different time steps. These models usually involve high computational costs, which make it difficult for them to optimise a large number of systems or to conduct parametric analyses. To avoid

* Corresponding author.
E-mail address: guillermo.alamo@ulpgc.es (G.M. Álamo).

https://doi.org/10.1016/j.oceaneng.2024.117802
Received 2 February 2024; Received in revised form 25 March 2024; Accepted 4 April 2024
Available online 9 April 2024

Nomenclature

Δ	Nondimensional roughness (–)
α_{ch}	Relative length of chord (–)
α_w	Angle between the wind direction and element axis (rad)
$\beta_{br,A\vee B}$	Relative diameter of brace A or B (–)
η	Requirement utilisation factor (–)
γ_M	Material factor (–)
γ_{ch}	Diameter to thickness ratio of chord (–)
Λ_1	Scalar parameter of longitudinal turbulence (m)
λ_{wind}	Scale parameter of the Weibull distribution of wind (m/s)
ν_s	Poisson's ratio of the soil (–)
ω	Angular frequency (rad/s)
ρ_a	Air density (kg/m^3)
ρ_w	Water density (kg/m^3)
σ_{ETM}	Standard deviation of wind turbulence in ETM (m/s)
$\sigma_{ETM,f_{KS}\geq f_{r,max}}$	Standard deviation of wind turbulence above $f_{r,max}$ in ETM (m/s)
σ_{NTM}	Standard deviation of wind turbulence in NTM (m/s)
$\sigma_{NTM,f_{KS}\geq f_{r,max}}$	Standard deviation of wind turbulence above $f_{r,max}$ in NTM (m/s)
$\sigma_{a0,Sd}$	Design axial compression stress (N/m^2)
$\sigma_{mi,Sd}$	Maximum design bending stress about given axis (N/m^2)
σ_v	Equivalent von-Mises stress (N/m^2)
$\tau_{br,A\vee B}$	Relative thickness of brace A or B (–)
$\theta_{br,A\vee B}$	Angle of brace A or B (°)
ξ_{ae}	Aeroelastic damping ratio (–)
$\xi_{ae,FA}$	Aeroelastic damping ratio in fore-aft direction (–)
$\xi_{ae,SS}$	Aeroelastic damping ratio in side-side direction (–)
ξ_n	Equivalent viscous damping (–)
ζ_{br}	Relative gap between braces (–)
A_h	Factor to account for cyclic or static loading condition (–)
A_p	Gross end area of the pile (m^2)
A_R	Wind turbine rotor area (m^2)
A_s	Side surface area of the pile (m^2)
C^a	Punctual aeroelastic damper (N s/m)
C_A	Added mass coefficient (–)
C_D	Drag coefficient (–)
C_M	Mass coefficient (–)
C_T	Thrust coefficient of the wind turbine (–)
D	Diameter (m)
D_{bottom}	Wind turbine tower bottom diameter (m)
$D_{br,A\vee B}$	Diameter of brace A or B (m)
D_{br_i}	Diameter of bracing tubular members of level i (m)
D_{ch}	Diameter of chord (m)
D_{leg}	Diameter of legs tubular members (m)
D_{pile}	Pile diameter (m)
D_{rotor}	Rotor diameter (m)
D_{top}	Wind turbine tower top diameter (m)
E_{pile}	Young's modulus of the pile (N/m^2)
EOG	Extreme operating gust
ETM	Extreme turbulence model
f_{akd}	Design local buckling strength (N/m^2)
f_{Ei}	Euler buckling strength about given axis (N/m^2)
$\mathbf{F}_{ext}$	External forces vector (N, N m)
F_H	Lateral force on pile head (N)
f_{kcd}	Design column buckling strength (N/m^2)
f_{KS}	Wind turbulence frequency in Kaimal spectrum (Hz)
f_n	Natural frequency (Hz)
$f_{r,max}$	Rotor maximum rotation speed (Hz)
$f_{r,min}$	Rotor minimum rotation speed (Hz)
f_{RO}	Wind turbine operating excitation frequencies (Hz)
f_s	Unit skin friction capacity (Pa)
F_{TH}	Wind thrust force on the wind turbine rotor (N)
f_{th}	Sectional thrust force owing to wind on elements above sea level (N/m)
f_{wn}	Sectional normal force owing to sea on submerged elements (N/m)
$f_{wn}^{current}$	Sectional normal force owing to current velocity (N/m)
f_{wn}^{eq}	Sectional normal force owing to sea including dynamic amplification (N/m)
f_y	Elastic strength of the material (N/m^2)
$\hat{f}$	Complex natural frequency (Hz)
g	Acceleration of gravity (m/s^2)
g_{br}	Gap between braces (m)
G_s	Shear modulus of the soil (N/m^2)
$H_{ESS,1}$	Wave height of 1-y extreme sea state (m)
$H_{ESS,50}$	Wave height of 50-y extreme sea state (m)
$H_{EWH,1}$	1-y extreme wave height (m)
$H_{EWH,50}$	50-y extreme wave height (m)
H_{jck}	Height of the jacket structure (m)
H_{tower}	Height of the wind turbine tower (m)
H_w	Water depth (m)
h_{wave}	Wave height (m)
I_{pile}	Pile cross-section moment of inertia (m^4)
I_{ref}	Expected value of turbulence intensity for 15 m/s (–)
$I_{RNA,roll}$	Rotor-nacelle assembly moment of inertia about roll axis (kg m^2)
$I_{RNA,yaw}$	Rotor-nacelle assembly moment of inertia about yaw axis (kg m^2)
$\mathbf{K}$	Static stiffness matrix (N/m, N, N m)
K^{eq}	Equivalent stiffness of the fundamental mode of the fixed-base wind turbine (N/m)

this drawback, Jalbi and Bhattacharya (2020) proposed a simplified methodology for estimating the axial forces in tubular members, assuming a truss structure. This procedure is useful for obtaining the first approximation of a design, without verifying the feasibility of the structure.

The influence of the soil–structure interaction (SSI) on the response of specific jacket structures for OWTs has been studied recently. Abdullahi et al. (2020) analysed the variations in the natural frequencies

$\mathbf{K}_{f,f}$	Stiffness submatrix of external forces on the foundation link due to foundation link displacements (N/m, N, N m)
$\mathbf{K}_{f,j}$	Stiffness submatrix of external forces on the foundation link due to jacket structure displacements (N/m, N, N m)
k_h	Initial modulus of soil's subgrade reaction (N/m^3)
$\mathbf{K}_{j,f}$	Stiffness submatrix of external forces on the jacket structure due to foundation link displacements (N/m, N, N m)
$\mathbf{K}_{j,j}$	Stiffness submatrix of external forces on the jacket structure due to jacket structure displacements (N/m, N, N m)
$\mathbf{K}_{SSI}$	Foundation impedance matrix (N/m, N, N m)
k_{wave}	Wave number (m^{-1})
k_{wind}	Shape parameter of the Weibull distribution of wind (–)
$\tilde{\mathbf{K}}$	Complex stiffness (and damping) matrix (N/m, N, N m)
L_{ch}	Length of chord (m)
L_{pile}	Pile length (m)
$\mathbf{M}$	Mass matrix (kg, kg m, kg m^2)
M_H	Bending moment on pile head (N m)
M_{jck}	Mass of the jacket foundation (kg)
M_{RNA}	Rotor-nacelle assembly mass (kg)
m_w	Sectional added mass owing to water–structure interaction (kg/m)
n_{br}	Number of bracing levels of the jacket (–)
n_{leg}	Number of legs of the jacket (–)
NTM	Normal turbulence model
p_s	Sectional reaction of soil (N/m)
p_u	Sectional ultimate bearing capacity of soil (N/m)
Q_p	Total end-bearing resistance (N)
q_p	Unit end-bearing capacity (Pa)
Q_s	Skin friction resistance (N)
Q_u	Ultimate axial bearing capacity (N)
S_{base}	Legs spacing at the base of the jacket (m)
S_{top}	Legs spacing at the top of the jacket (m)
T	Thickness (m)
t	Time (s)
T_{bottom}	Wind turbine tower bottom thickness (m)
$T_{br,A\vee B}$	Thickness of brace A or B (m)
T_{br_i}	Thickness of bracing tubular members of level i (m)
T_{ch}	Thickness of chord (m)
T_{leg}	Thickness of legs tubular members (m)
T_{pile}	Pile thickness (m)
T_{top}	Wind turbine tower top thickness (m)
T_{wave}	Wave period (s)
$\mathbf{u}$	Nodal displacements vector (m, rad)
u_{avg}	Average annual wind speed at hub (m/s)
u_{e50}	Extreme wind speed with a 50-y recurrence period (m/s)
u_m	Mean component of the wind speed at hub (m/s)
U_{out}	Cut-out wind speed of wind turbine (m/s)
u_p	Lateral pile deflection (m)
U_R	Rated wind speed of wind turbine (m/s)
u_{tb}	Turbulent component of the wind speed at hub (m/s)
u_{wind}	Wind velocity (m/s)
$v_{c,circ}$	Circulational current velocity (m/s)
$v_{c,wind}$	Wind generated current velocity (m/s)
v_n	Normal component of water particle velocity (m/s)
$\dot{v}_n$	Normal component of water particle acceleration (m/s^2)
w_i	Radial basis functions weights (–)
X	Jacket design variables included in the optimisation process (–)
x	Horizontal distance in the waves propagation direction (m)
X_{c_i}	Radial basis functions centres (–)
z	Vertical position measured above sea level (m)
z_p	Depth measured from the mud line (m)
z_{ref}	Vertical position (z) taken as reference (m)

of an OWT on monopile and jacket structures while considering the flexibility of the pile foundation. Sharmin et al. (2017) compared the seismic response of a jacket-supported OWT in different soils and on a rigid base, where the SSI was found to be of great relevance. Shi et al. (2015) investigated the effect of the lateral flexibility of a pile foundation on the internal forces in certain elements of a predefined jacket structure under design loads. They used a Winkler spring model to incorporate the SSI, although the vertical component was not considered. However, few authors have incorporated the effects of foundation flexibility in the optimisation of jacket structures. One example is the work of Ju and Hsieh (2022), who implemented nonlinear springs along a buried pile to incorporate foundation flexibility. However, the relevance of including SSI effects in jacket structure analysis models to obtain more efficient and less expensive designs has not been studied in depth.

The objective of this study was to analyse the influence of SSI phenomena on the structural evaluation of jacket foundations for OWTs. For this purpose, an optimisation process was conducted to obtain feasible jacket designs, for which a significant analysis of the impact of foundation flexibility on the structural response and feasibility criteria was performed. To accelerate jacket optimisation, a model for the evaluation of structural feasibility was introduced, which offered simplifications that reduced the computational cost without a significant loss of accuracy. A reduced set of the most representative load states was established, and a static equivalent analysis was conducted to introduce all the relevant environmental loads, accounting for the effects of foundation flexibility. The structural response of the jacket foundation was obtained, and the main verifications required for this type of structure were evaluated according to international standards. Section 2 describes the structural typology of the jacket and presents a general formulation of the structural optimisation problem. Section 3 describes the numerical model used to determine the structural response of the jacket, including the design loads and requirements imposed by international standards. Section 4 presents the designs obtained from the optimisation process and how they are influenced by the SSI. Finally, the main conclusions of this study are summarised in Section 5.

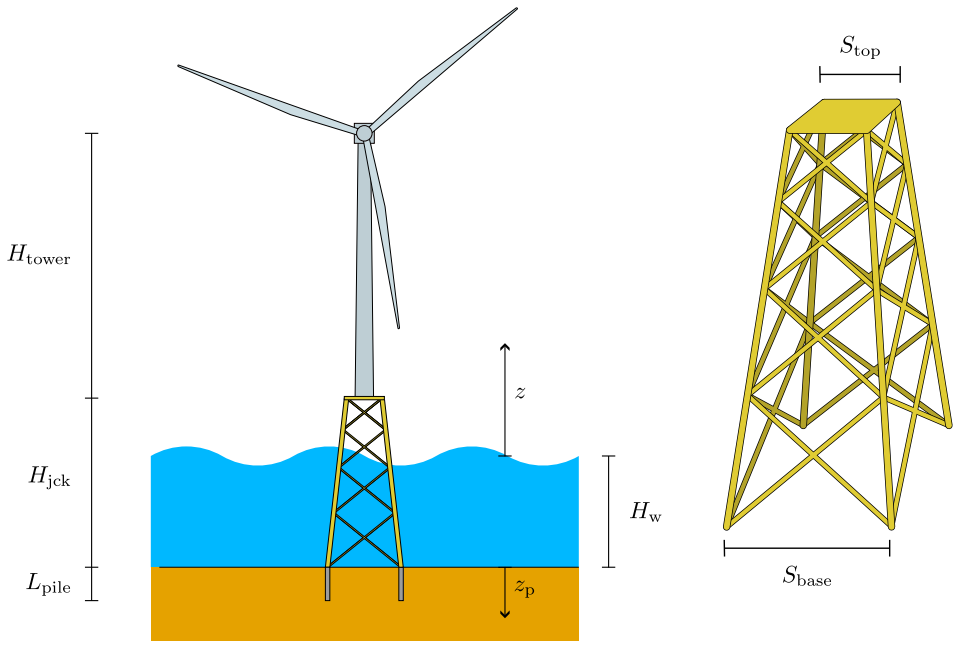

Fig. 1. Representation of an offshore wind turbine on a jacket support structure with four legs and four levels of bracing, all with the same inclination.

2. Problem statement

A jacket foundation is a three-dimensional structure composed of tubular elements welded as a frame structure, as shown in Fig. 1. The geometry of this structure is typically reduced to three or four legs joined by different levels of bracing, which provide stability.

From a general perspective, the system topology can be defined by the following set of hyperparameters: the height of the structure (H_{jck}), number of legs (n_{leg}), number of bracings (n_{br}) and their spacing, and separation of the legs at the base (S_{base}) and top (S_{top}). Regarding cross-sections, note that the geometries of several elements must coincide to provide radial symmetry to the structure. The structural assembly is fixed to the seabed using foundation elements connected to the bottom of the legs of the structure. A pile foundation was assumed in this study.

To study the relevance of the SSI in this type of structure, it is necessary to analyse whether significant differences appear in the response of the structure when considering this interaction compared to the rigid base assumption. However, the large number of variables defining the structure makes it unviable to conduct a parametric study that exhaustively considers all possible configurations. For this reason, this study proposed an optimisation process that allows feasible jacket designs for a wind turbine and specific environmental conditions to be obtained to test the relevance of SSI phenomena in relevant systems.

To obtain the jacket design, it was necessary to define the case study described in Section 4.1. First, the characteristics of the wind turbine must be specified, including both the physical properties, such as the mass and geometry of the tower, and the operating conditions of the device. Then, the environmental conditions of the site where the system is located, which include the depth of the sea, wave and wind conditions, and geotechnical characteristics, were also required because they affect the requirements that the jacket structure must verify.

Once the characteristics of the case study were defined, optimisation was performed. The specific procedure is detailed in Section 4.2. The objective of this process is to obtain a feasible jacket design that minimises the amount of material used, which is a significant economic cost. Therefore, the total mass of the structure was established as a cost function. In addition, some restrictions were imposed to avoid the failure of the structure or structural elements against external loads (ultimate limit states [ULS]), ensure the correct functionality of the system (serviceability limit states [SLS]), avoid the collapse of the structure owing to cyclic loads (fatigue limit states [FLS]), and limit the geometry of certain elements under technical criteria. Therefore, if the lower and upper limits are considered to limit the search space, the following optimisation problem under inequality constraints can be established:

$$\begin{aligned} &\text{Minimise} && M_{\text{jck}}(X) \\ &\text{subject to} && X \geq \text{lower limit} \\ & && X \leq \text{upper limit} \\ & && \eta_j(X) \leq 1,\ j = 1, \ldots, n \end{aligned} \tag{1}$$

where M_{jck} is the mass of the jacket foundation, X represents the variables modified in the optimisation process, and η is the utilisation factor of the constraint j. This factor is used to transform the generic expressions of the inequality constraints into dimensionless and uniform inequalities by dividing the two terms of the inequality; thus, the requirement is fulfilled if its value is equal to or less than 1. This new indicator allows a distinct comparison of the closeness of the evaluated design to the restrictions imposed on each check.

The structural model presented in Section 3 was used to evaluate all established requirements. This model implemented the calculation and structural evaluation of the jacket, including several acceptable simplifications to reduce the computational cost to be used in the optimisation process. As expected, the results of the optimisation process were affected by the hypothesis considered in the connection of the base of the leg with the soil. This study aimed to show the direction and its relevance. The strategy consisted of performing the optimisation process under two assumptions: considering the SSI and imposing the bottom legs on a fixed base (FB). Once the jacket designs were obtained under both considerations, the structural model was used to evaluate the utilisation factors of the imposed requirements on the jacket under the same hypothesis with which it was obtained and the other. Fig. 2 shows the combination of designs and hypotheses used to compare the results. These results are shown in Section 4.3.

3. Structural model

The proposed evaluation model incorporated the most relevant loads on the support jacket structure and considered a reduced set of representative load states. Moreover, a structural analysis was performed using a finite element model with acceptable simplifications.

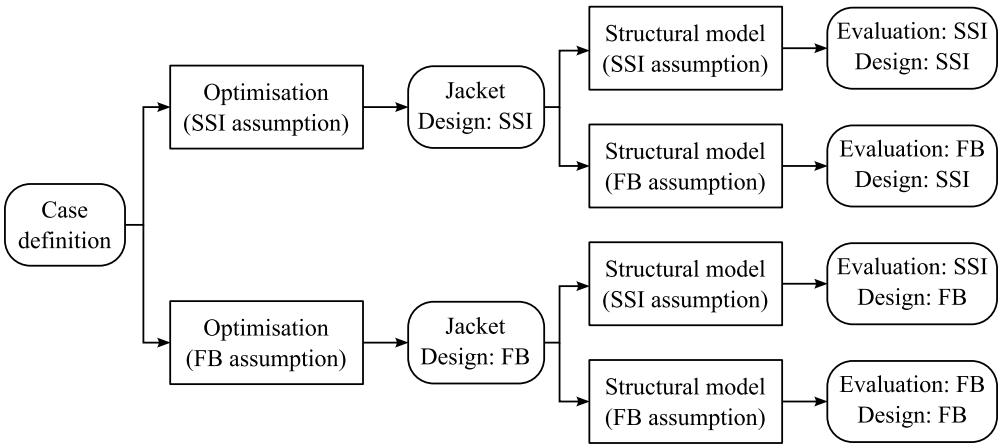

Fig. 2. Diagram of the overall process of SSI relevance analysis. Designs obtained under each hypothesis are evaluated using both.

Details of the model are presented in this section. Fig. 3 shows a flow diagram of all the processes implemented in the model and the information flow. This information flow is represented by arrows that start with the corresponding input variables or outputs of the intermediate processes, and end with the process that requires this information.

3.1. Design loads

The jacket structure must support permanent loads derived from gravitational action, and variable loads caused mainly by the action of meteorological and hydrological phenomena. International standards include all loads that must be considered in the design. However, this model included the most relevant loads for determining the design of this type of foundation, as described in this section.

3.1.1. Permanent loads

The permanent loads considered in this study were limited to gravitational loads. First, the self-weight was considered as a distributed vertical load for all the tubular members of the jacket structure. The platform and wind turbine weights were considered as punctual vertical loads applied to the centre of the jacket top platform.

The other contribution was the hydrostatic pressure on the submerged elements, which produced buoyancy forces. Considering the hydrostatic pressure produced by water, punctual loads at the nodes owing to the pressure on the free faces of the section and a normal sectional load distributed along the element owing to the pressure gradient in the section were considered.

3.1.2. Environmental load scenarios

DNV codes (DNV GL AS, 2016a) contain numerous load combinations that must be verified in OWT designs. Evaluating all of them in an approximate procedure such as the one proposed herein would increase the computational cost of the process and reduce the advantages of its use. Therefore, the environmental loads implemented in this model were reduced to those derived from the action of wind and sea, which are known to be the most frequent and significant in this type of offshore structure. The five load hypotheses proposed by Arany et al. (2017) were adopted as the most significant hypotheses for the proposed evaluation model. The load states listed in Table 1 are based on different combinations of wind and waves. The wind conditions were as follows.

- **U1 - Normal turbulence scenario:** The average wind speed is equal to the rated wind speed (U_R) under a normal turbulence model **(NTM)**.
- **U2 - Extreme turbulence scenario:** The average wind speed is equal to the rated wind speed (U_R) under an extreme turbulence model **(ETM)**.

Table 1
Load states considered in the presented model, proposed by Arany et al. (2017).

Scenario	Wind model	Wave model	Alignment	Limit state
E1	NTM at U_R (U1)	1-y ESS (W1)	Collinear	ULS and SLS
E2	ETM at U_R (U2)	50-y EWH (W4)	Collinear	ULS and SLS
E3	EOG at U_R (U3)	1-y EWH (W2)	Collinear	ULS and SLS
E4	EOG at U_{out} (U4)	50-y EWH (W4)	Collinear	ULS and SLS
E5	ETM at U_R (U2)	50-y EWH (W4)	Misaligned 90°	ULS and SLS

- **U3 - Extreme gust at rated wind speed scenario:** The average wind speed is equal to the rated wind speed (U_R) under the 50-y extreme operating gust **(EOG)**.
- **U4 - Extreme gust at cut-out scenario:** The average wind speed is equal to the cut-out wind speed (U_{out}) under the 50-y extreme operating gust **(EOG)**.

Conversely, the conditions related to waves are

- **W1 - 1-y extreme sea state:** A stationary wave scenario with a 1-y significant wave height.
- **W2 - 1-y extreme wave height:** A stationary wave scenario with a 1-y maximum wave height.
- **W3 - 50-y extreme sea state:** A Stationary wave scenario with a 50-y significant wave height.
- **W4 - 50-y extreme wave height:** A stationary wave scenario with a 50-y maximum wave height.

The expressions needed to evaluate these scenarios are summarised in subsequent sections.

3.1.3. Wind loads

The main component of wind action is the load on the wind turbine rotor. This can be simplified as

$$F_{TH} = \frac{1}{2}\,\rho_a\,A_R\,C_T\,\left(u_m + u_{tb}\right)^2 \tag{2}$$

where A_R represents the wind turbine rotor area, u_m and u_{tb} are the mean and turbulent components of the wind speed, respectively, and C_T is the thrust coefficient used by Arany et al. (2017).

$$C_T = \begin{cases} \dfrac{3.5\,(2\,u_m + 3.5)}{u_m^2} & u_m \le U_R \\ \dfrac{3.5\,U_R\,(2\,U_R + 3.5)}{u_m^3} & U_R < u_m \le U_{out} \end{cases} \quad ; \quad \text{being } C_T \le 1 \tag{3}$$

where U_R and U_{out} are the rated and cut-out wind speeds of the wind turbine, respectively.

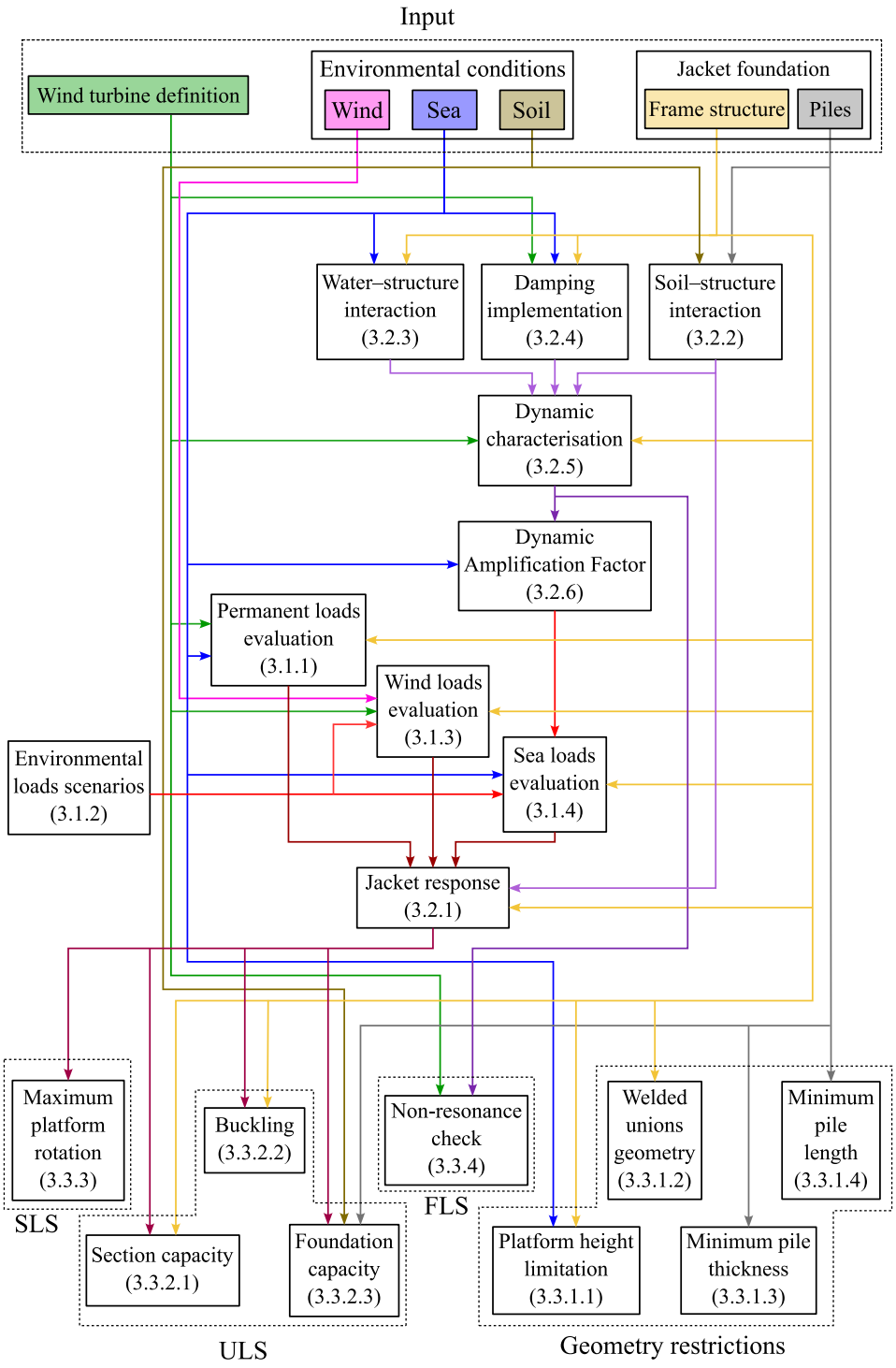

Fig. 3. Flow diagram of the calculation process implemented in the model. Arrows connect the input variables or intermediate results with the processes that require that information. The numbers in brackets indicate the paper sections in which each process is detailed.

In addition, the wind load acting on the structural elements located above sea level was considered. In this case, a distributed load was implemented along the element according to DNVGL-RP-C205 (DNV GL AS, 2017a).

$$f_{\text{th}} = \frac{1}{2} C_{\text{D}} D \rho_{\text{a}} \sin(\alpha_{\text{w}}) u_{\text{wind}}(z)^2 \tag{4}$$

where C_{D} represents the drag coefficient (defined in Eq. (15)), α_{w} the angle between the wind direction and the element axis, and u_{wind} is the wind velocity, which depends on the height (z):

$$u_{\text{wind}}(z) = u_{\text{wind}}(z_{\text{ref}}) \left(\frac{z}{z_{\text{ref}}} \right)^{0.12} \tag{5}$$

To evaluate this load in the different load cases, the mean speed (u_{m}) was considered to be the one that characterises the load state (Table 1), whereas the turbulent speed (u_{tb}) was estimated from the associated wind model (defined by IEC-61400-1 IEC, 2005).

- **Normal turbulence model (NTM)**
The standard deviation presented by the wind turbulence under this model is defined as

$$\sigma_{\mathrm{NTM}} = I_{\mathrm{ref}} \left(0.75\, u_{\mathrm{m}} + 5.6\right) \tag{6}$$

where I_{ref} is the expected value of the turbulence intensity at 15 m/s, which depends on the class of the wind turbine. In this study, a value of 0.16 was taken as it was the most critical case. In a real wind turbine, it must be understood that the pitch control will modify the blade orientation, and with it, the drag coefficient. Therefore, turbulence with a sufficiently low frequency of variation should not be included in this calculation because there would be a different load hypothesis at another wind speed. It was assumed that the frequency limit that the pitch control could not correct was the maximum rotor speed ($f_{\mathrm{r,max}}$) (Arany et al., 2017). The Kaimal spectrum (Kaimal et al., 1972) was used to recalculate the standard deviation of turbulence:

$$\begin{aligned}\sigma_{\mathrm{NTM},f_{\mathrm{KS}}\geq f_{\mathrm{r,max}}} &= \sigma_{\mathrm{NTM}} \sqrt{\int_{f_{\mathrm{r,max}}}^{\infty} \frac{\frac{4{\cdot}8.1\Lambda_1}{u_{\mathrm{m}}}}{\left(1+\frac{6{\cdot}8.1\Lambda_1}{u_{\mathrm{m}}} f_{\mathrm{KS}}\right)^{\frac{5}{3}}}\, \mathrm{d}f_{\mathrm{KS}}} \\ &= \sigma_{\mathrm{NTM}} \sqrt{\frac{1}{\left(1+\frac{6{\cdot}8.1\Lambda_1}{u_{\mathrm{m}}} f_{\mathrm{r,max}}\right)^{\frac{2}{3}}}}\end{aligned} \tag{7}$$

where Λ_1 is the scalar parameter of longitudinal turbulence,

$$\Lambda_1 = \begin{cases} 0.7\, z & z \leq 60\,\mathrm{m} \\ 42 & z \geq 60\,\mathrm{m} \end{cases} \tag{8}$$

Given that the IEC-61400-1 (IEC, 2005) standard establishes the 90% percentile as a representative value for this turbulence model, the turbulent component of speed would be

$$u_{\mathrm{tb}} = 1.282\, \sigma_{\mathrm{NTM},f_{\mathrm{KS}}\geq f_{\mathrm{r,max}}} \tag{9}$$

- **Extreme turbulence model (ETM)**
The procedure for obtaining the turbulent component of the velocity in the extreme turbulence model is similar to that of the normal turbulence model. In this case, the standard deviation also depends on the annual average wind velocity at the hub level (u_{avg}), as indicated by the following expression:

$$\sigma_{\mathrm{ETM}} = 2\, I_{\mathrm{ref}} \left(0.072 \left(\frac{u_{\mathrm{avg}}}{2}+3\right)\left(\frac{u_{\mathrm{m}}}{2}-4\right)+10\right) \tag{10}$$

The same procedure as in Eq. (7) was applied, and the representative value for turbulence was established at the 95% percentile.

$$u_{\mathrm{tb}} = 1.645\, \sigma_{\mathrm{ETM},f_{\mathrm{KS}}\geq f_{\mathrm{r,max}}} \tag{11}$$

- **Extreme operating gust (EOG)**
In the case of the extreme operating gust, the turbulent component of wind velocity is defined by the following expression:

$$u_{\mathrm{tb}} = \min\left\{1.35\left(0.8\, u_{\mathrm{e50}} - u_{\mathrm{m}}\right);\ \frac{3.3\,\sigma_{\mathrm{NTM}}}{1+\frac{D_{\mathrm{rotor}}}{10\,\Lambda_1}}\right\} \tag{12}$$

where σ_{NTM} is defined by Eq. (6), Λ_1 by Eq. (8), D_{rotor} is the rotor diameter, and u_{e50} is the reference wind speed, which is established by the class of the wind turbine and is defined as the mean value of 10 min of the extreme wind speed at the height of the hub, with a recurrence period of 50 y. Because this reference data is generally not available, following DNVGL-RP-C205 (DNV GL AS, 2017a), its value was estimated from the characterisation of the wind in the area:

$$u_{\mathrm{e50}} = \lambda_{\mathrm{wind}} \left(-\ln\left(1-\sqrt[52560]{0.98}\right)\right)^{\frac{1}{k_{\mathrm{wind}}}} \tag{13}$$

where λ_{wind} and k_{wind} are the scale and shape parameters of the Weibull distribution of wind velocity, respectively.

3.1.4. Sea load

A drag force perpendicular to the element was considered for the submerged elements of the jacket. The tangential component was neglected. According to DNVGL-RP-C205 (DNV GL AS, 2017a), the force received by the structural element can be evaluated as follows:

$$f_{\mathrm{wn}} = \rho_{\mathrm{w}}\, C_{\mathrm{M}}\, \frac{\pi\, D^2}{4}\, \dot{v}_{\mathrm{n}} + \frac{1}{2}\, \rho_{\mathrm{w}}\, C_{\mathrm{D}}\, D\, |v_{\mathrm{n}}|\, v_{\mathrm{n}} \tag{14}$$

where v_{n} and $\dot{v}_{\mathrm{n}}$ are the normal components of the water particle velocity and acceleration, respectively, C_{M} is the mass coefficient (taken as 2 for safety reason), and C_{D} is the drag coefficient, which is obtained via

$$C_{\mathrm{D}} = \begin{cases} 0.65 & \Delta \leq 10^{-4} \\ (29+4\,\log(\Delta))/20 & 10^{-4} < \Delta \leq 10^{-2} \\ 1.05 & \Delta > 10^{-2} \end{cases} \quad \text{being } \Delta = 5\cdot 10^{-6}/D \tag{15}$$

The water particle velocity and acceleration fields were defined through the superposition of the wave and current models. Both models were extracted from DNVGL-RP-C205 (DNV GL AS, 2017a).

- **Current model:**
The implemented current model assumed constant velocities; therefore, its contribution to the acceleration field was neglected. The velocity of the water particles was obtained from the superposition of the wind-generated and circulational currents:

  - Wind-generated current: This was modelled by a linear profile from the water surface to a depth of 50 m. The induced speed on the surface corresponded to 3% of the wind speed at a height of 10 m.

$$v_{\mathrm{c,wind}}(z) = v_{\mathrm{c,wind}}(0)\left(\frac{z+50}{50}\right) \quad \text{for } -50\,\mathrm{m} \leq z \leq 0 \tag{16}$$

  - Circulational currents: The tidal current velocity profile along water depth (H_{w}) was considered. The particle velocity on the surface was assumed to represent current environmental data.

$$v_{\mathrm{c,circ}}(z) = v_{\mathrm{c,circ}}(0)\left(\frac{z+H_{\mathrm{w}}}{H_{\mathrm{w}}}\right)^{\frac{1}{7}} \quad \text{for } z \leq 0 \tag{17}$$

- **Wave model**
To define the water particle velocity and acceleration fields completely, it was necessary to determine the wave period. According to DNVGL-ST-0437 (DNV GL AS, 2016a), the wave period in deep water can be assumed to be within the following range:

$$11.1\sqrt{\frac{h_{\mathrm{wave}}}{g}} \leq T_{\mathrm{wave}} \leq 14.3\sqrt{\frac{h_{\mathrm{wave}}}{g}} \tag{18}$$

From this interval, the lower limit can be assumed to be the period of the wave in the calculation, because it is the worst-case scenario. The velocity and acceleration fields can then be defined according to the Airy wave theory.

$$v_{\mathrm{w,x}} = \frac{\pi\, h_{\mathrm{wave}}}{T_{\mathrm{wave}}} \frac{\cosh\left(k_{\mathrm{wave}}\left(z+H_{\mathrm{w}}\right)\right)}{\sinh\left(k_{\mathrm{wave}}\, H_{\mathrm{w}}\right)} \cos\left(k_{\mathrm{wave}}\, x - \frac{2\pi}{T_{\mathrm{wave}}}\, t\right) \tag{19a}$$

$$v_{\mathrm{w,z}} = \frac{\pi\, h_{\mathrm{wave}}}{T_{\mathrm{wave}}} \frac{\sinh\left(k_{\mathrm{wave}}\left(z+H_{\mathrm{w}}\right)\right)}{\sinh\left(k_{\mathrm{wave}}\, H_{\mathrm{w}}\right)} \sin\left(k_{\mathrm{wave}}\, x - \frac{2\pi}{T_{\mathrm{wave}}}\, t\right) \tag{19b}$$

$$\dot{v}_{\mathrm{w,x}} = \frac{2\,\pi^2\, h_{\mathrm{wave}}}{T_{\mathrm{wave}}^2} \frac{\cosh\left(k_{\mathrm{wave}}\left(z+H_{\mathrm{w}}\right)\right)}{\sinh\left(k_{\mathrm{wave}}\, H_{\mathrm{w}}\right)} \sin\left(k_{\mathrm{wave}}\, x - \frac{2\pi}{T_{\mathrm{wave}}}\, t\right) \tag{19c}$$

$$\dot{v}_{\mathrm{w,z}} = -\frac{2\,\pi^2\, h_{\mathrm{wave}}}{T_{\mathrm{wave}}^2} \frac{\sinh\left(k_{\mathrm{wave}}\left(z+H_{\mathrm{w}}\right)\right)}{\sinh\left(k_{\mathrm{wave}}\, H_{\mathrm{w}}\right)} \cos\left(k_{\mathrm{wave}}\, x - \frac{2\pi}{T_{\mathrm{wave}}}\, t\right) \tag{19d}$$

where k_{wave} is the wave number obtained by solving the following implicit equation:

$$\frac{2\pi}{k_{wave}} = T_{wave}\sqrt{\frac{g}{k_{wave}}\tanh\left(k_{wave}\,H_w\right)} \tag{20}$$

3.2. Numerical model for structural analysis

The proposed model performed an equivalent static analysis of the jacket response under external forces. However, the dynamic characterisation of the system is a fundamental aspect for the feasibility evaluation of the structure. Therefore, the dynamic effects of the water–structure interaction, damping, and SSI were introduced for this calculation.

3.2.1. Jacket substructure response

To analyse the static response of the jacket foundation, the wind turbine and its loads were replaced by the loads transferred to the jacket. This is mechanically allowed because the wind turbine forms an isostatic subsystem, and the efforts at the tower base depend only on the loads and not on the displacements. Nevertheless, this element must be included in the dynamic characterisation described in Section 3.2.5. A linear finite element model was implemented to obtain the response of the jacket structure under the loads described in Section 3.1. For each load case, the following system of equations was solved:

$$\mathbf{K}\cdot\mathbf{u} = \mathbf{F}_{ext} \tag{21}$$

Where $\mathbf{F}_{ext}$ represents the vector of the external forces acting on the structure, $\mathbf{K}$ is the stiffness matrix of the system, and $\mathbf{u}$ is the nodal displacement.

The structural elements were modelled using Timoshenko beam theory (Friedman and Kosmatka, 1993), considering a rigid connection between the elements in the welded unions. The platform was considered to be rigid, linking the nodes of the upper legs.

All the external forces applied to the wind turbine and the weight of the platform were transformed into an equivalent system of forces applied on the central node located at the top of the jacket structure, whereas the external forces on the jacket were considered as trapezoid-distributed loads. Nontrapezoidal distributed loads, such as wave loads from sea states, were discretised into sufficient trapezoidal intervals to approximate the variability of the loads along the elements, and each interval was computed as an independent trapezoidal load.

3.2.2. Soil–structure interaction

SSI was considered by including the foundation stiffness in the stiffness matrix of the structure,

$$\mathbf{K} = \begin{bmatrix} \mathbf{K}_{j,j} & \mathbf{K}_{j,f} \\ \mathbf{K}_{f,j} & \mathbf{K}_{f,f} + \mathbf{K}_{SSI} \end{bmatrix} \tag{22}$$

where $\mathbf{K}_{a,b}$ represent the stiffness submatrices related to the jacket ($\square_j$) or foundation link ($\square_f$) nodes, and $\mathbf{K}_{SSI}$ is the impedance matrix of the foundation (which can include all the effects related to stiffness, damping, and inertia relevant in the resonance frequency calculation in Section 3.2.5). In general, the impedance matrix of the foundation contains all the terms corresponding to the lateral, torsional, and axial modes of the piles, as well as the coupled terms representing the pile–soil–pile interaction. This model allows the implementation of different impedance functions to reproduce the SSI. In this study, the stiffness of the pile foundation was obtained from an available numerical model (Álamo et al., 2016) based on the integral formulation of the pile–soil interaction with Green's function of the layered half-space and by modelling the piles as beam elements. This model reproduced the three-dimensional linear elastic response of a group of piles embedded in soil. The impedance matrix obtained through this model contained all terms corresponding to the individual pile response and pile-to-pile interaction of the lateral (horizontal, rocking, and swaying) and axial (vertical) modes. No torsional interaction was considered between the individual piles and the surrounding soil. In the case of a static analysis (such as that described in Section 3.2.1), this impedance matrix was reduced only to the foundation stiffness.

However, the proposed model can also neglect any SSI effect by considering the bottom of the legs to be completely fixed (that is, the rigid base assumption).

3.2.3. Water–structure interaction

To consider the water–structure interaction phenomena, the distributed mass of the submerged elements was increased for the transverse displacements by the following term:

$$m_w = \rho_w\frac{\pi\,(D-2T)^2}{4} + C_A\,\rho_w\frac{\pi\,D^2}{4} \tag{23}$$

where C_A is the added mass coefficient, which is typically considered to be 1. Eq. (23) shows two different terms. The first is attributed to the mass contained inside the structural element (in case it was filled with water), and the second is associated with the interaction with the surrounding water, which was established according to DNV-RP-C205 (DNV GL AS, 2017a).

3.2.4. Damping

Four sources of damping of the dynamic system were included in the proposed model.

- Frequency-independent material damping was considered, and the hysteretic damping coefficient was used to define a complex-valued Young's modulus.
- Energy dissipation by the water–structure interaction was simplified as an increase in the damping of the material of the submerged tubular elements.
- Energy dissipation by the SSI was introduced by the imaginary component of the impedance matrix added to the system.
- Aeroelastic damping was incorporated as a local hysteric frequency-independent damper into the rotor shaft. The damping coefficient was obtained as $C^a = 2\,\xi_{ae}\,K^{eq}$ from the considered aeroelastic damping ratio for the device (ξ_{ae}) and the equivalent stiffness corresponding to the fundamental mode of the wind turbine founded on a rigid base (K^{eq}). Owing to the particular dynamic characteristics of this system, the equivalent stiffness value could be approximated using the static stiffness at the rotor height. Once the local damping was determined, it was applied to the rotor node of the complete system, where the wind turbine was supported by the jacket structure. A representation of this is shown in Fig. 4.

3.2.5. Dynamic characterisation

To obtain a dynamic characterisation of the structural system, it was necessary to incorporate a wind turbine into the finite element model. For this, the tower was discretised into a sufficient number of elements with a uniform section so that it was capable of reproducing its tapered geometry, and it was linked to the upper central node of the jacket structure. With respect to the mass of the system, a mass matrix was constructed to collect the inertial behaviour of the tubular elements of the jacket and the water–structure interaction (Section 3.2.3). In addition, the mass and inertias of the rotor-nacelle assembly (RNA) and the mass of the platform were introduced as punctual masses and inertias.

The natural frequencies of the system were obtained by solving the eigenvalue problem $\left(\left|\tilde{\mathbf{K}} - \omega^2\mathbf{M}\right| = 0\right)$. When the SSI interaction model is frequency-dependent, this procedure must be solved iteratively while updating the impedance values.

Because damping was introduced into the system through complex terms in the stiffness matrix, the natural frequencies obtained were

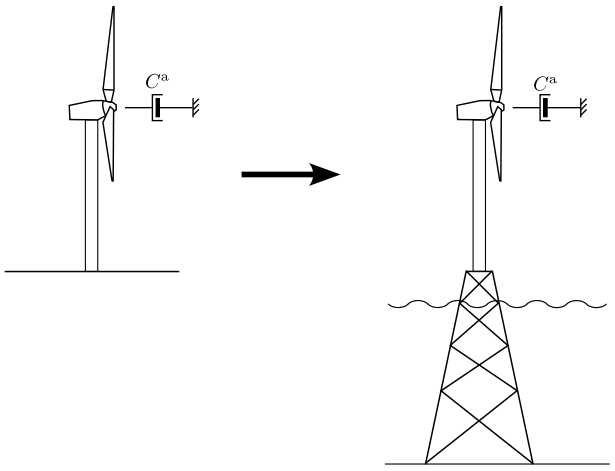

Fig. 4. Representation of the extrapolation of the aeroelastic damping produced in the rotor of the wind turbine considered on a fixed base in the system with the wind turbine on the jacket foundation.

complex. Therefore, the values of the real natural frequency and damping of the system were obtained through an analogy of a system of one degree of freedom using the following expressions:

$$f_n = |\hat{f}| \tag{24a}$$

$$\xi_n = \frac{\mathrm{Im}\left(\hat{f}\right)}{|\hat{f}|} \tag{24b}$$

where $\hat{f}$ represents the complex frequency obtained by the eigenvalue, f_n is the natural frequency of the system, and ξ_n is the equivalent viscous damping of the vibration mode.

3.2.6. Equivalent static analysis

The structural response was evaluated using an equivalent static analysis, as indicated by Eq. (21). However, the considered environmental loads exhibited time dependence, which had to be adequately addressed. Wind loads are assumed to vary over long periods of time; therefore, they can be directly considered as static loads.

However, the wave load presents a significant oscillation over short periods of time, which can induce dynamic effects on the structure that increase the stresses to which it is subjected. Therefore, following the recommendation of Arany et al. (2017), the contribution of the waves to the sea load was increased by the following dynamic amplification factor (DAF):

$$\mathrm{DAF} = \frac{1}{\sqrt{\left(1 - \left(\frac{1}{T_{\mathrm{wave}}\, f_n}\right)^2\right)^2 + \left(\frac{2\,\xi_n}{T_{\mathrm{wave}}\, f_n}\right)^2}} \tag{25}$$

where T_{wave} represents the period of the wave excitation, f_n is the natural frequency of the system, and ξ_n is the mode damping. For the conservative approach, the highest amplification factor among the different vibration modes was obtained. Because the sea load was obtained from the nonlinear superposition of the wave (periodic) and current (static) velocity fields, the DAF value was only applied to the dynamic component of the sea load, that is, the difference between the total sea load and the load obtained only because of the current velocity field:

$$f_{\mathrm{wn}}^{\mathrm{eq}} = f_{\mathrm{wn}}^{\mathrm{current}} + \mathrm{DAF}\left(f_{\mathrm{wn}} - f_{\mathrm{wn}}^{\mathrm{current}}\right) \tag{26}$$

In addition to the dynamic amplification effects, wave oscillation induces a significant variation in the magnitude and direction of sea loads (Eq. (19)). To account for this variation and ensure that the jacket structure is evaluated at a critical instant in the wave cycle, different phases of the wave cycle must be considered and verified.

Table 2
Load factor (DNV GL AS, 2016a).

	ULS (Favourable)	ULS (Unfavourable)	SLS
Permanent loads	0.90	1.10	1.00
Environmental loads	1.35	1.35	1.00

To collect the load variability accurately, 15 independent load states were included for each sea state, with their phases homogeneously distributed throughout the wave cycle.

3.3. Design principles

The requirements that jacket foundations should fulfil, established by international standards, are detailed in this section. According to their characteristics, the restrictions can be geometric, with some limitations imposed on the dimensions of the structural elements or the assembly according to technical criteria, or failure, which are the criteria that determine the integrity and functionality of the structural assembly. This last group is divided into ULS, SLS, and FLS. Structural analysis is required to determine the forces, displacements, and dynamic characterisation of the jacket foundation.

To determine the effects of external loads on the structure, a partial factor safety method was used to obtain the target safety level. For the material factor (γ_M), DNVGL-ST-0126 (DNV GL AS, 2016b) recommends taking a value of 1.1 for tubular structures, whereas the load factor can be found in DNVGL-ST-0437 (DNV GL AS, 2016a). Table 2 lists the values considered for each load type depending on the required check. To reduce the calculation, and assuming that it is sufficiently secure, a value of 1.1 was considered for the different ULS checks in permanent loads.

3.3.1. Geometric requirements

Platform height. Jacket platforms for offshore support structures do not need to be designed to resist direct wave impacts. Therefore, the height of the platform should be set to be sufficient to overcome the largest expected waves, including the air gap. This air gap must be at least 20% of the wave height, but with a minimum value of 1 m, according to DNVGL-ST-0126 (DNV GL AS, 2016b).

$$H_{\mathrm{jck}} \geq H_{\mathrm{w}} + \frac{H_{\mathrm{EWH,50}}}{2} + \max\{0.2\, H_{\mathrm{ESS,50}}, 1\} \tag{27}$$

where H_{w} represents the maximum expected depth of water, $H_{\mathrm{EWH,50}}$ is the 50-y extreme wave height, and $H_{\mathrm{ESS,50}}$ is the 50-y extreme sea state.

Welded unions. Geometric restrictions were imposed on the joints to achieve viable structures from a constructive perspective. These limits were taken from Appendix B of DNVGL-RP-C203 (DNV GL AS, 2016c). Based on the variables defined in Fig. 5, the dimensionless parameters were defined, as shown in Eq. (28). The adopted intervals are indicated in Eq. (29).

$$\beta_{\mathrm{br,A\vee B}} = D_{\mathrm{br,A\vee B}} / D_{\mathrm{ch}} \tag{28a}$$

$$\alpha_{\mathrm{ch}} = 2\, L_{\mathrm{ch}} / D_{\mathrm{ch}} \tag{28b}$$

$$\tau_{\mathrm{br,A\vee B}} = T_{\mathrm{br,A\vee B}} / T_{\mathrm{ch}} \tag{28c}$$

$$\zeta_{\mathrm{br}} = g_{\mathrm{br}} / D_{\mathrm{ch}} \tag{28d}$$

$$\gamma_{\mathrm{ch}} = D_{\mathrm{ch}} / \left(2\, T_{\mathrm{ch}}\right) \tag{28e}$$

$$0.2 \leq \beta_{\mathrm{br,A\vee B}} \leq 1 \tag{29a}$$

$$4 \leq \alpha_{\mathrm{ch}} \tag{29b}$$

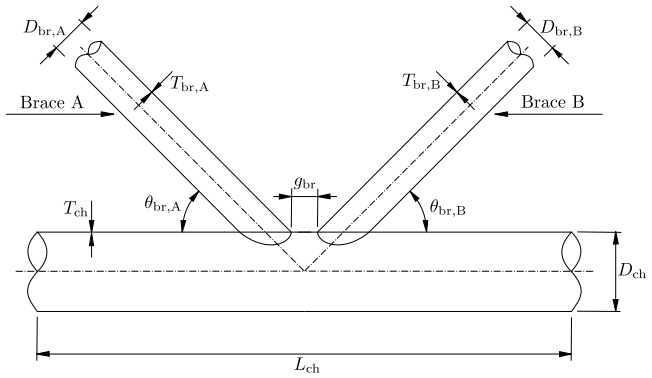

Fig. 5. Geometric variables considered in the joints. *Source:* Adapted from DNVGL-RP-C203 (DNV GL AS, 2016c).

$$0.2 \leq \tau_{br,A\vee B} \leq 1 \tag{29c}$$

$$0.6\,\beta_{br,A\vee B} / \sin\left(\theta_{br,A\vee B}\right) \leq \zeta_{br} \leq 1 \tag{29d}$$

$$8 \leq \gamma_{ch} \leq 32 \tag{29e}$$

$$20^\circ \leq \theta_{br,A\vee B} \leq 90^\circ \tag{29f}$$

Minimum pile thickness. To ensure that the pile foundation resists the loads derived from the installation process, API Recommended Practice 2A-WSD (API, 2007) indicates that the thickness of the pile should be

$$T_{pile} \geq \frac{6.35}{1000} + \frac{D_{pile}}{100} \tag{30}$$

Embedded length of pile. Following the recommendation of Arany et al. (2017), a lower limit was included for the length of the pile, such that its critical length was reached. For this purpose, the expression proposed by Randolph (1981) was used:

$$L_{pile} \geq D_{pile}\left(\frac{E_{pile}\frac{64\,I_{pile}}{\pi\,D_{pile}^4}}{G_s\left(1+\frac{3}{4}\nu_s\right)}\right)^{\frac{2}{7}} \tag{31}$$

where I_{pile} and E_{pile} are the moment of inertia of the pile cross-section and Young's modulus of its material, respectively, and G_s and ν_s are the shear modulus and Poisson's ratio of the soil, respectively.

3.3.2. Ultimate limit states (ULS)

Section capacity. Given that it is an elastic material, the von Mises yield criterion was used to evaluate the resistance capacity of the section. This equivalent stress (σ_v) must be less than or equal to the elastic strength of the material (f_y) reduced by the factor of the material (γ_M).

$$\sigma_v \leq \frac{f_y}{\gamma_M} \tag{32}$$

Buckling. Buckling-failure modes must be verified. For this purpose, the column buckling strength was assessed for each beam element between the two welded joints, according to Section 3.8 of DNVGL-RP-C202 (DNV GL AS, 2017b). To avoid the evaluation of joint stiffness and assuming that it is safer, the effective length factor was taken to be equal to 1, as if all joints were pinned connections. The stability requirement for a shell column subjected to axial compression and bending is given by

$$\frac{\sigma_{a0,Sd}}{f_{kcd}} + \frac{1}{f_{akd}}\sqrt{\left(\frac{\sigma_{m1,Sd}}{1-\frac{\sigma_{a0,Sd}}{f_{E1}}}\right)^2 + \left(\frac{\sigma_{m2,Sd}}{1-\frac{\sigma_{a0,Sd}}{f_{E2}}}\right)^2} \leq 1 \tag{33}$$

where $\sigma_{a0,Sd}$ is the design axial compression stress, $\sigma_{mi,Sd}$ is the maximum design bending stress about a given axis, f_{akd} is the design local buckling strength, f_{kcd} is the design column buckling strength, and f_{Ei} is the Euler buckling strength. However, an analysis of the global buckling modes must be conducted to ensure structural stability.

Also, the shell buckling stability for unstiffened circular cylinders was checked according to Section 3.4 of DNVGL-RP-C202 (DNV GL AS, 2017b).

Foundation capacity. To evaluate the capacity of the pile foundation, API Recommended Practice 2A-WSD (API, 2007) was followed. For this purpose, an auxiliary model based on nonlinear Winkler springs was used to reproduce the lateral pile–soil interaction according to the standard. Fig. 6 represents the model used, where a sufficient number of distributed springs were defined, assuming that the soil around the pile is sand, and the lateral resistance–deflection (p–y) relation is as follows:

$$p_s = A_h\,p_u\,\tanh\left(\frac{k_h\,z_p}{A_h\,p_u}\,u_p\right) \tag{34}$$

where p_u is the ultimate bearing capacity at depth z_p, k_h is the initial modulus of the subgrade reaction, u_p is the lateral deflection, and A_h is a factor taken as 0.9 if cyclic loading conditions are assumed.

Independent of the SSI model used in the structural analysis (Section 3.2.2), the loads that equilibrated the jacket structure at the bottom node of the legs were considered and used as the head loads of each pile (F_H, M_H). To evaluate the pile, two planes of the forces that were assumed to be most relevant were considered: the plane with the highest lateral force and the corresponding bending moment, and the plane with the highest bending moment and the corresponding lateral force.

Two failure criteria were established to verify the capacity of the foundation: the pile yield and soil resistance. The first implies that the tensile stress produced by the maximum bending moment along the pile cannot exceed the yield stress limit. The latter ensures that the soil can resist the loads induced by the pile without becoming unstable. This condition is checked by defining different amplification-reduction factors of the lateral load and bending moment at the pile head and determining the case in which the displacement of the pile head tends to infinity, which would indicate the maximum lateral force the soil could support.

The axial bearing capacity of the piles was also evaluated by comparing the axial forces at each pile head against the ultimate bearing capacity of the piles, following API Recommended Practice 2A-WSD (API, 2007), computed as

$$Q_u = Q_s + Q_p = f_s\,A_s + q_p\,A_p \tag{35}$$

where Q_s is the skin friction resistance obtained by multiplying the unit skin friction capacity (f_s) by the side surface area of the pile (A_s), and Q_p is the total end-bearing resistance, evaluated as the unit end-bearing capacity (q_p) multiplied by the gross end area of the pile (A_p). The values of these areas depend on whether the pile is assumed to be plugged or unplugged. For plugged piles, the side surface area of the pile is limited to the external area, whereas the entire bottom cross section is considered for the gross end area. However, for unplugged piles, only the pile annular area acts on the end-bearing capacity, and the inner wall surface is also incorporated to compute the frictional resistance. Once the values for both hypotheses were computed, the smallest value was considered as the pile's ultimate axial bearing capacity. Finally, for the pullout bearing capacity, the foundation resistance was provided by the total skin friction, together with the effective weight of the pile and the assumed soil plug.

3.3.3. Serviceability limit states (SLS)

To ensure correct operation of the wind turbine, DNVGL-ST-0126 (DNV GL AS, 2016b) recommends a maximum limit rotation at the bottom of the tower. In this case, a limit of 0.25° was applied to the jacket platform.

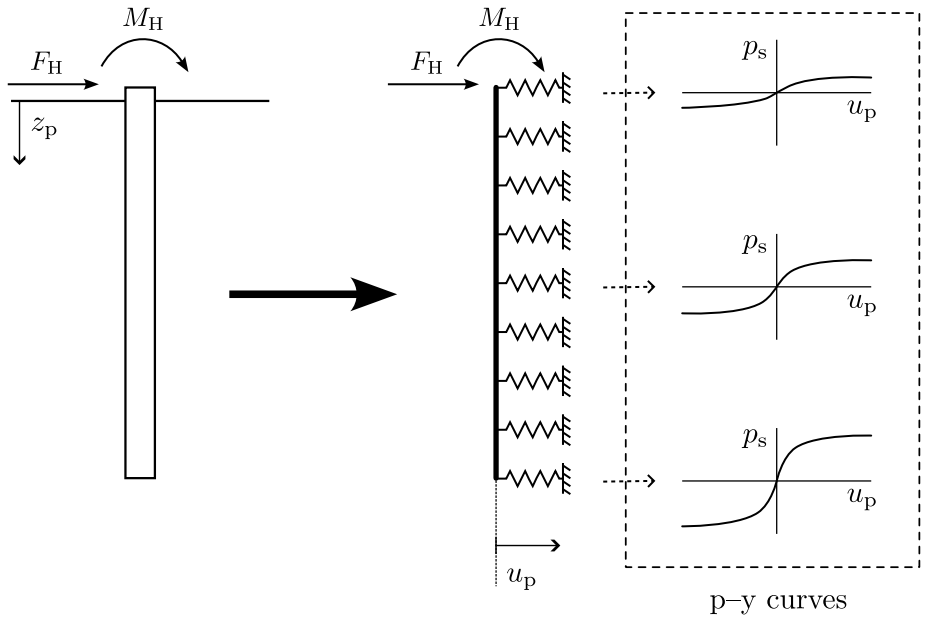

Fig. 6. Representation of static Winkler model used for the evaluation of lateral foundation capacity.

3.3.4. Fatigue limit states (FLS)

To reduce the risk of long-term material fatigue failure, DNVGL-ST-0126 (DNV GL AS, 2016b) states that the natural frequencies of a structural assembly cannot coincide with the rotor speed or blade frequency to avoid resonance. The following conditions should be fulfilled:

$$\frac{f_{RO}}{f_n} \leq 0.95 \quad \text{or} \quad \frac{f_{RO}}{f_n} \geq 1.05 \tag{36}$$

where f_{RO} represents the frequencies to avoid (all bandwidths of the rotor speed and blade transition frequency), and f_n are the different natural frequencies of the structure. This code also indicates that, to verify this condition, all natural frequencies at least 20% higher than the blade transition frequency must be obtained.

4. Results

As shown in this section, the optimisation procedure mentioned in Section 2 was performed to obtain a jacket design considering two cases: (1) accounting for the SSI and (2) assuming a fixed base (FB) for the bottom legs. Next, all the designs obtained were evaluated under both assumptions to analyse the relevance of SSI phenomena. To achieve an acceptable computational cost for this process, the structural model presented in Section 3 was used to evaluate the technical requirements.

4.1. Case study

The selected wind turbine was a DTU 10-MW reference wind turbine (Bak et al., 2013). According to the characteristics of the proposed model, the properties of the device necessary to evaluate the structure are those that define the geometry of the tower (tower height, bottom and top diameters, and bottom and top thicknesses), inertia provided by the RNA (mass and moments of inertia about the roll and yaw axes), aeroelastic damping of the rotor (in the fore-aft and side-side directions), rotor diameter, and operation conditions (rated wind speed and rotor velocities). Table 3 lists the properties and their values, adapted from Bak et al. (2013). The values of aeroelastic damping were assumed from the intervals proposed by Chen and Duffour (2018). It was assumed that the tower and tubular elements of the jacket were composed of steel and had the following properties: density of 7850 kg/m^3, Young's modulus of 210 GPa, Poisson's ratio of 0.3, hysteretic damping coefficient of 0.5%, and yield stress of 350 MPa.

Table 3
Wind turbine properties.
Source: Adapted from Bak et al. (2013).

Variable	Value
Tower height (H_{tower})	119 m
Rotor diameter (D_{rotor})	178.3 m
Bottom diameter (D_{bottom})	8.3 m
Bottom thickness (T_{bottom})	0.038 m
Top diameter (D_{top})	5.5 m
Top thickness (T_{top})	0.02 m
Mass (M_{RNA})	$674 \cdot 10^3$ kg
Inertia about roll axis ($I_{RNA,roll}$)	$156 \cdot 10^6$ kg m^2
Inertia about yaw axis ($I_{RNA,yaw}$)	$974 \cdot 10^5$ kg m^2
Fore-aft direction damping ($\xi_{ae,FA}$)	6%
Side-side direction damping ($\xi_{ae,SS}$)	0.75%
Rated wind speed (U_R)	11.4 m/s
Minimum rotor speed ($f_{r,min}$)	6 rpm
Maximum rotor speed ($f_{r,max}$)	9.6 rpm

The environmental conditions at the site where the wind turbine is located must be also defined. Wind conditions were defined by a Weibull distribution with an average speed of 10 m/s and a shape parameter of 1.8. For the metocean data, those described by Jalbi and Bhattacharya (2020) were taken, where the variables were a water depth of 50 m, a 1-y significant wave height of 6.6 m, a 1-y maximum wave height of 12.42 m, a 50-y significant wave height of 8.27 m, and a 50-y maximum wave height of 15.33 m; the circulational current was neglected. In addition, it was assumed that in the submerged structural elements of the jacket, the damping of the material increased by one percentage point.

Finally, the jacket structure was assumed to be founded on sand, defined as a homogeneous soil with a Young's modulus of 25 MPa, a Poisson's ratio of 0.49, a density of 2000 kg/m^3, a hysterical damping ratio of 2.5%, and an angle of internal friction of 30°.

4.2. Jacket optimisation

Next, a jacket support structure was designed by considering the SSI. Some assumptions were made to simplify the process and reduce the dimensions of the optimisation problem. First, the height of the

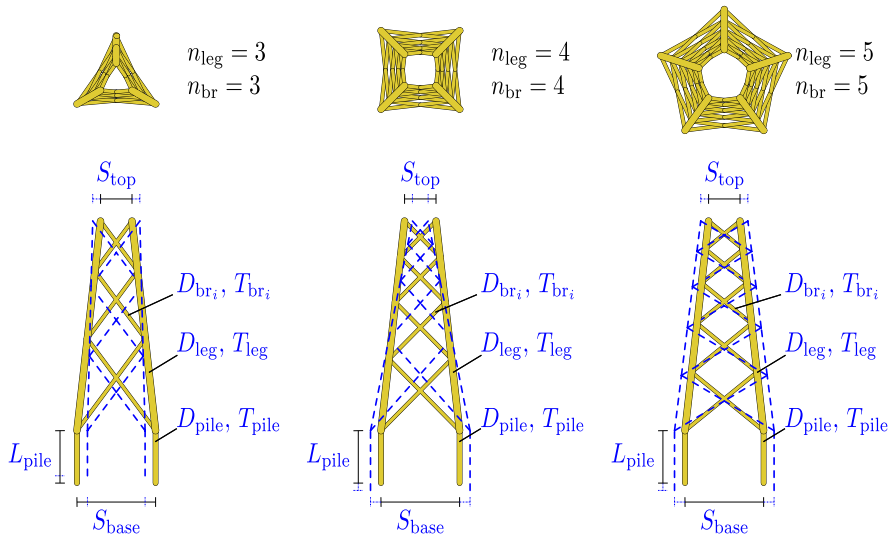

Fig. 7. Representation of three examples of jacket designs indicating the variables included (blue) or fixed (black) in the optimisation process.

Table 4
Ranges of the expressions considered in the design process. The jacket design variables are obtained from these expressions.

Expression	Lower limit	Upper limit
n_{leg}	3	5
n_{br}	2	10
S_{base}	15 m	35 m
$\frac{S_{top} - D_{bottom} \cdot \tan(\pi/n_{leg})}{S_{bottom} - D_{bottom} \cdot \tan(\pi/n_{leg})}$	0	1
D_{leg}	0.6 m	2.5 m
T_{leg}/D_{leg}	1/64	1/16
D_{pile}	0.8 m	4 m
T_{pile}/D_{pile}	1/80	1/4
L_{pile}/D_{pile}	8	18
D_{br_i}/D_{leg}	0.2	1
T_{br_i}/D_{br_i}	1/64	1/16

jacket was fixed at 59.3 m, which was the minimum value allowed according to Eq. (27). All bracing elements were assumed to have the same inclination. Regarding the grouping of the geometry of the different tubular elements, all the elements of each bracing level had the same cross-section, all the legs were uniform through their lengths and equal, and all the piles had the same dimensions. Finally, the design of the jacket platform was neglected. It was directly considered as a punctual mass equivalent to a 20-cm-thick steel plate that would fill the polygon defined by the upper extremes of the legs.

In this way, the design variables of this problem were as follows: the number of legs (n_{leg}), the number of bracing levels (n_{br}), the separation of the legs at the base (S_{base}) and top (S_{top}), the diameter (D_{leg}) and thickness (T_{leg}) of the legs, the diameter (D_{br_i}) and thickness (T_{br_i}) of the elements of each bracing level (i), and the diameter (D_{pile}), thickness (T_{pile}), and length (L_{pile}) of the piles. However, the number of legs and bracing levels were excluded from the optimisation process because they are discrete variables, resulting in a different design for each combination. Fig. 7 shows a schematic representation of the optimisation variables. To limit the solution search space, many of the design variables were not directly used but were defined from dimensionless ratios. The relationships between the design variables and their ranges are presented in Table 4.

The jacket design was obtained by solving the optimisation problem in Eq. (1). Owing to the large number of optimisation processes conducted in this study, a surrogate was used to reduce the total number of evaluations of the structural model and the total computational cost (Negrin et al., 2023). The optimisation procedure based on the "surrogateopt" function already implemented in MATLAB (Matlab, 2020) was used, which created an internal surrogate model adapted from model evaluations and sped up the process. This surrogate model was based on interpolation using radial basis functions, which consists of a linear combination of radially symmetric functions centred at defined points.

$$L_{RBF}(X) = \sum_{i=1}^{n} w_i \, \varphi\left(X, X_{c_i}\right) \tag{37}$$

where φ is the radial basis function, X_{c_i} are the centres of the function, and w_i are the weights of the functions. Setting the already evaluated points as centres, the weight values were obtained using least squares to construct the interpolation function. First, the optimisation process generated random points and evaluated them to build the initial surrogate models for both the objective function and nonlinear constraints. These interpolation functions were used to evaluate numerous random points. From this, a new point to be evaluated by the structural model was selected by considering the expected performance given by the surrogate model and the distance from previously known points. The surrogate model was then updated, and the process was repeated until the stopping criterion was met.

To achieve a balance between obtaining an acceptable design and a fast procedure, the number of model evaluations in each execution of the MATLAB function was limited to 100. Next, the "surrogateopt" function was applied iteratively, introducing the accumulated evaluations as previously evaluated points until the mass of the obtained solution did not reduce the previous one by more than 1%. This procedure was followed for each of the established combinations of the numbers of legs and bracing levels, performing five repetitions of each to estimate the convergence of the process. In addition, a linear buckling analysis was applied to all the results to ensure the structural stability of the obtained designs.

Fig. 8 shows the masses of the obtained designs grouped by the numbers of legs and bracing levels. To do this, the cases were separated on the x-axis according to the number of bracing levels; red crosses were used for three-legged jackets, blue squares for four-legged jackets, and green diamonds for five-legged jackets. These results show that there were significant differences in the global mass among the five designs obtained for each combination of the numbers of legs and

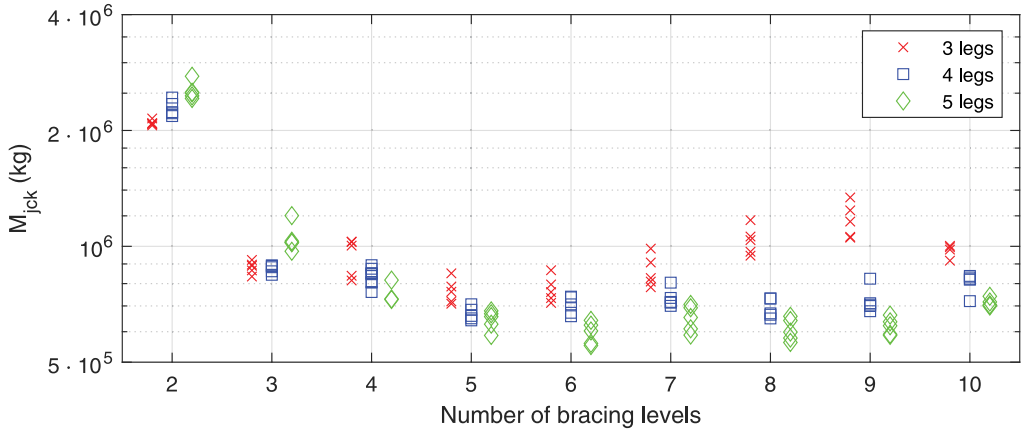

Fig. 8. Mass of jackets obtained in the design process, differentiated by the numbers of legs (markers) and bracing levels.

bracing levels. This indicates that the design process does not guarantee the optimal design of the jacket structure; however, the implementation of more rigorous optimisation procedures would significantly increase the computational cost and is outside the scope of this study. However, general trends can be observed from Fig. 8. First, the mass of the structure tended to decrease as the number of bracing levels increased, until six bracing levels were reached. From that point onwards, a slight increase in the mass of the assembly was observed, which was more sensitive when the structure had fewer legs. The structures obtained with four or more bracing levels became lighter as the number of legs increased.

To determine the optimal jacket design, it is necessary to select the design that verifies all imposed requirements and imposes a lower economic cost. However, many researchers use the global mass of the jacket as a function to minimise in the optimisation process of these structures (see, for example, Chew et al., 2016; Oest et al., 2017; Couceiro et al., 2020; Ju and Hsieh, 2022). This is mainly owing to the complexity and variability of estimating the cost of such structural systems, which have a high number of joints. For this reason, the process is usually simplified by considering the mass of the assembly, because the amount of material required is a main factor affecting the final cost. Considering these criteria, and according to the results shown in Fig. 8, the selected range of jacket designs in this problem can be limited to four-legged cases that have between four and six bracing levels, because lower values in these variables imply a significant growth in the global mass of the structure, and higher values imply an increase in costs owing to the increase in the number of welded joints. Table 5 lists the dimensions of five lighter jackets obtained within this range.

Table 5
Values of the design variables of the five selected jackets.

	Design 1	Design 2	Design 3	Design 4	Design 5
n_{leg}	4	4	4	4	4
n_{br}	5	5	6	5	6
S_{base} (m)	27.96	28.61	25.33	30.85	27.45
S_{top} (m)	14.63	12.94	15.28	12.63	12.77
D_{leg} (m)	0.984	1.015	1.071	0.971	1.077
T_{leg} (mm)	42.88	48.15	43.29	47.33	45.49
D_{pile} (m)	2.552	2.398	2.393	2.644	2.540
T_{pile} (mm)	31.9	30.3	30.3	33.1	31.8
L_{pile} (m)	30.9	31.6	34.1	28.0	28.5
D_{br_1} (m)	0.484	0.406	0.430	0.504	0.362
T_{br_1} (mm)	10.1	16.0	9.3	11.4	12.9
D_{br_2} (m)	0.404	0.416	0.522	0.509	0.327
T_{br_2} (mm)	12.0	10.4	12.0	9.9	14.4
D_{br_3} (m)	0.344	0.391	0.358	0.664	0.336
T_{br_3} (mm)	13.5	12.4	10.6	12.0	18.8
D_{br_4} (m)	0.746	0.557	0.342	0.415	0.667
T_{br_4} (mm)	13.2	17.4	9.1	21.9	17.2
D_{br_5} (m)	0.614	0.546	0.433	0.658	0.336
T_{br_5} (mm)	21.4	18.9	14.6	13.8	14.5
D_{br_6} (m)	–	–	0.653	–	0.509
T_{br_6} (mm)	–	–	23.4	–	23.4
M_{jck} (kg)	$642 \cdot 10^3$	$650 \cdot 10^3$	$658 \cdot 10^3$	$659 \cdot 10^3$	$672 \cdot 10^3$

4.3. Influence of the soil–structure interaction

Next, the influence of the SSI on the design of the jacket structure was analysed. To achieve this, the same design procedure was followed, but the bottom legs were considered to be on a fixed base (FB). To prevent unrealistic designs from modifying the conclusions drawn from this study, designs with four legs and four, five, and six levels of bracing were selected, as they were considered more efficient according to the results of Section 4.2.

Fig. 9 shows a boxplot of the utilisation factors (defined in Section 2), which reflect the safety level with different restrictions imposed on each of the designs obtained. First, the results showed that all the values obtained were less than one because they were obtained from a design process that verified all the restrictions. Thus, the criteria in which the indicators presented values close to 1 were those that limited the final dimensions of the jacket. In the case of designs considering the SSI, the ULS in the bracings and the limitation of the rotation of the tower base of the wind turbine were the most restrictive requirements, whereas when the legs were considered on a fixed base, the ULS in the bracings and load capacity of the foundation were the most relevant restrictions.

To evaluate the influence of the SSI model on the utilisation factors, the designs obtained considering the SSI were evaluated assuming a rigid base and vice versa. Fig. 10 shows boxplots of the utilisation factors, where the top left and bottom right subplots are the same as those in Fig. 9. Restrictions associated with the geometry of the welded unions, the thickness of the pile, and the critical length of the pile were omitted because they are purely geometric restrictions that are not affected by the numerical model used to evaluate the structure. The failure criterion that was most affected by the foundation assumption was the rotation at the base of the tower because considering the SSI made the structure more flexible and increased the displacements. However, this criterion was not relevant, because it is a recommendation of the DNV (DNV GL AS, 2016b) and is not mandatory. Finally, when the

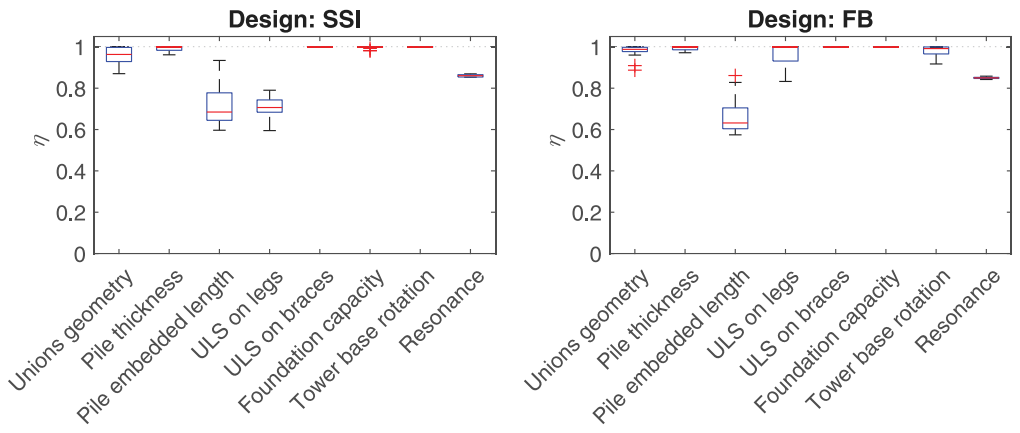

Fig. 9. Utilisation factors of jackets obtained in the design processes assuming soil–structure interaction effects (left) or a rigid base (right).

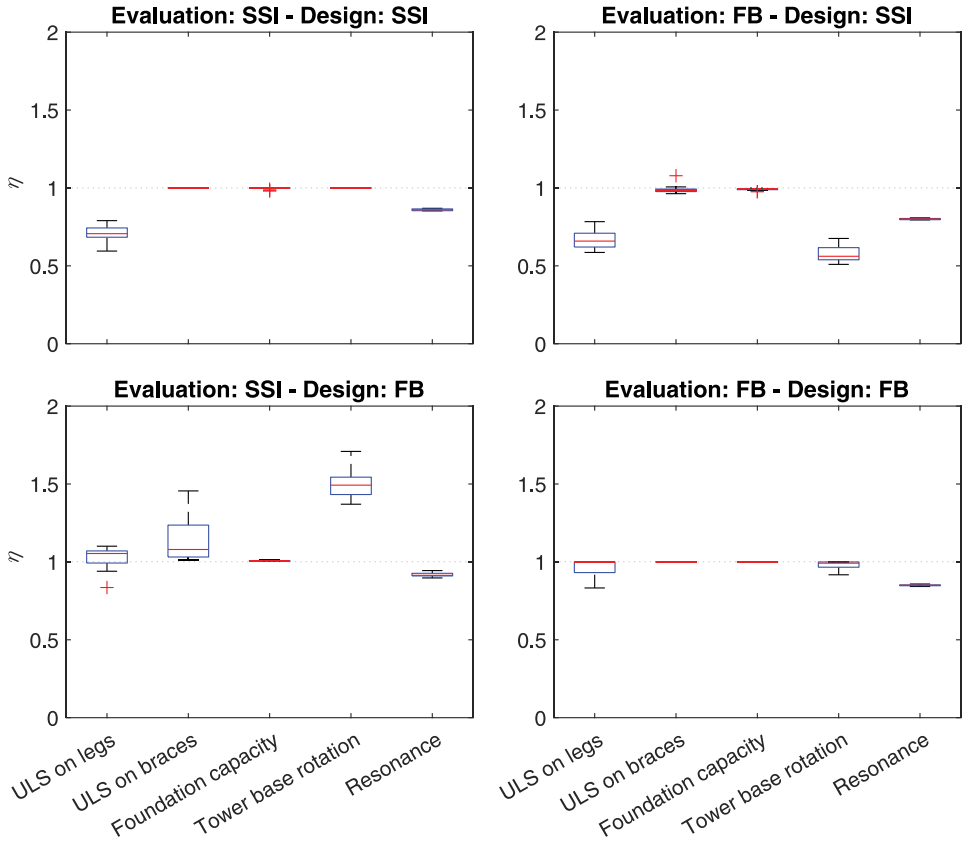

Fig. 10. Utilisation factors of jackets obtained in the design processes evaluated considering the soil–structure interaction (SSI) or a fixed base (FB).

designs obtained assuming a fixed base were evaluated considering the SSI, the ULS requirements for the legs and bracings of the jacket were not satisfied. This implies that the redistribution of efforts by considering foundation flexibility has significant relevance in the failure criteria of these structures, and therefore, should not be neglected.

5. Conclusions

This study proposed a first approach to analysing the influence of the SSI in the structural evaluation of jackets to support OWTs. An optimisation process was performed to obtain feasible jacket designs for a specific location and wind turbine, where the conclusions drawn are relevant. A structural model was necessary to measure the influence of the SSI and incorporate it into the optimisation process. The structural model was used to evaluate the most critical load cases acting on jacket-supported OWTs. In addition, it incorporated the verification of design principles that limit the topology of the structure, and failure principles that check the viability of the jacket from a structural perspective. The proposed approach is a compromise between extremely simplified methods and rigorous complex models, making it a suitable tool for the structural analysis of this type of complex structure using fewer computational resources.

The influence of the SSI was measured via the utilisation factors of the design requirements of the jackets evaluated considering the SSI but obtained assuming that the bottom legs were fixed and those evaluated considering the bottom legs to be fixed but obtained assuming the SSI.

ULS verifications in the legs and bracing elements were not satisfied when considering the SSI in designs obtained assuming a fixed base, whereas this did not occur significantly when evaluating fixed-base designs obtained with the SSI. It was concluded that the redistribution of internal forces produced by considering the flexibility of the foundation increases the stress on some structural elements, highlighting the need to incorporate this characteristic into structural models of OWT jacket support structures.

CRediT authorship contribution statement

Román Quevedo-Reina: Writing – review & editing, Writing – original draft, Visualization, Validation, Software, Methodology, Formal analysis, Conceptualization. **Guillermo M. Álamo:** Writing – review & editing, Supervision, Methodology, Conceptualization. **Stijn François:** Writing – review & editing, Supervision, Methodology, Conceptualization. **Geert Lombaert:** Writing – review & editing, Supervision, Methodology, Conceptualization. **Juan J. Aznárez:** Writing – review & editing, Project administration, Funding acquisition, Conceptualization.

Declaration of competing interest

The authors declare that they have no known competing financial interests or personal relationships that could have appeared to influence the work reported in this paper.

Data availability

Data will be made available on request.

Acknowledgements

This study was supported by the Ministerio de Ciencia e Innovación and the Agencia Estatal de Investigación of Spain (MCIN /AEI/10.13039/501100011033) through Research Project PID2020-120102RB-I00. In addition, R. Quevedo-Reina is a recipient of the FPU research fellowship (FPU19/04170) from the Ministerio de Universidades (MIU) of Spain, which also provided financial support for two short-term research stays at KU Leuven from 19 September 2022 to 18 December 2022 (EST22/00507) and from 4 September 2023 to 3 December 2023 (EST23/00392). This research was partially supported by ACIISI, Spain–Gobierno de Canarias and European ERDF Funds Grant EIS 2021 04.

References

Abdullahi, A., Wang, Y., Bhattacharya, S., 2020. Comparative modal analysis of monopile and jacket supported offshore wind turbines including soil-structure interaction. Int. J. Struct. Stab. Dyn. 20 (10), 2042016. http://dx.doi.org/10.1142/S021945542042016X.

Álamo, G., Martínez-Castro, A., Padrón, L., Aznárez, J., Gallego, R., Maeso, O., 2016. Efficient numerical model for the computation of impedance functions of inclined pile groups in layered soils. Eng. Struct. 126, 379–390. http://dx.doi.org/10.1016/j.engstruct.2016.07.047.

API, 2007. API RP 2A-WSD: Recommended practice for planning, designing and constructing fixed offshore platforms — Working stress design.

Arany, L., Bhattacharya, S., Macdonald, J., Hogan, S., 2017. Design of monopiles for offshore wind turbines in 10 steps. Soil Dyn. Earthq. Eng. 92, 126–152. http://dx.doi.org/10.1016/j.soildyn.2016.09.024.

Bak, C., Zahle, F., Bitsche, R., Kim, T., Yde, A., Henriksen, L., Natarajan, A., Hansen, M., 2013. Description of the DTU 10 MW reference wind turbine.

Chen, C., Duffour, P., 2018. Modelling damping sources in monopile-supported offshore wind turbines. Wind Energy 21 (11), 1121–1140. http://dx.doi.org/10.1002/we.2218.

Chew, K.-H., Tai, K., Ng, E., Muskulus, M., 2016. Analytical gradient-based optimization of offshore wind turbine substructures under fatigue and extreme loads. Mar. Struct. 47, 23–41. http://dx.doi.org/10.1016/j.marstruc.2016.03.002.

Couceiro, I., París, J., Navarrina, F., Guizán, R., Colominas, I., 2020. Optimization of offshore steel jackets: Review and proposal of a new formulation for time-dependent constraints. Arch. Comput. Methods Eng. 27 (4), 1049–1069. http://dx.doi.org/10.1007/s11831-019-09342-y.

DNV GL AS, 2016a. DNVGL-ST-0437: Loads and site conditions for wind turbines. URL http://www.dnvgl.com.

DNV GL AS, 2016b. DNVGL-ST-0126: Support structures for wind turbines.

DNV GL AS, 2016c. DNVGL-RP-C203: Fatigue design of offshore steel structures.

DNV GL AS, 2017a. DNVGL-RP-C205: Environmental conditions and environmental loads.

DNV GL AS, 2017b. DNVGL-RP-C202: Buckling strength of shells.

Friedman, Z., Kosmatka, J.B., 1993. An improved two-node timoshenko beam finite element. Comput. Struct. 47 (3), 473–481. http://dx.doi.org/10.1016/0045-7949(93)90243-7.

IEC, 2005. International Standard IEC-61400-1 wind turbines. Part 1: design requirements.

Jalbi, S., Bhattacharya, S., 2020. Concept design of jacket foundations for offshore wind turbines in 10 steps. Soil Dyn. Earthq. Eng. 139, http://dx.doi.org/10.1016/j.soildyn.2020.106357.

Ju, S., Hsieh, C., 2022. Optimal wind turbine jacket structural design under ultimate loads using Powell's method. Ocean Eng. 262, http://dx.doi.org/10.1016/j.oceaneng.2022.112271.

Kaimal, J.C., Wyngaard, J.C., Izumi, Y., Coté, O.R., 1972. Spectral characteristics of surface-layer turbulence. Q. J. R. Meteorol. Soc. 98 (417), 563–589. http://dx.doi.org/10.1002/qj.49709841707.

Matlab, 2020. Deep Learning Toolbox, Version 9.9.0.1592791 (R2020b) Update 5. The MathWorks Inc., Natick, Massachusetts.

Musial, W., Spitsen, P., Beiter, P., Duffy, P., Marquis, M., Cooperman, A., Hammond, R., Shields, M., 2021. Offshore Wind Market Report: 2021 Edition. Office of Energy Efficiency & Renewable Energy.

Negrin, I., Kripka, M., Yepes, V., 2023. Metamodel-assisted design optimization in the field of structural engineering: A literature review. Structures 52, 609–631. http://dx.doi.org/10.1016/j.istruc.2023.04.006.

Oest, J., Sørensen, R., Overgaard, L.C.T., Lund, E., 2017. Structural optimization with fatigue and ultimate limit constraints of jacket structures for large offshore wind turbines. Struct. Multidiscip. Optim. 55 (3), 779–793. http://dx.doi.org/10.1007/s00158-016-1527-x.

Randolph, M.F., 1981. The response of flexible piles to lateral loading. Géotechnique 31 (2), 247–259. http://dx.doi.org/10.1680/geot.1981.31.2.247.

Sharmin, F., Hussan, M.I.T., Kim, D., Cho, S.G., 2017. Influence of soil-structure interaction on seismic responses of offshore wind turbine considering earthquake incident angle. Earthq. Struct. 13, 39–50.

Shi, W., Park, H.C., Chung, C.W., Shin, H.K., Kim, S.H., Lee, S.S., Kim, C.W., 2015. Soil-structure interaction on the response of jacket-type offshore wind turbine. Int. J. Precis. Eng. Manuf. Green Technol. 2 (2), 139–148. http://dx.doi.org/10.1007/s40684-015-0018-7.

Stolpe, M., Wandji, W., Natarajan, A., Shirzadeh, R., Kühn, M., Kaufer, D., 2017. Innovative design of a 10MW steel-type jacket 308974.

Wang, L., Kolios, A., Liu, X., Venetsanos, D., Cai, R., 2022. Reliability of offshore wind turbine support structures: A state-of-the-art review. Renew. Sustain. Energy Rev. 161, 112250. http://dx.doi.org/10.1016/j.rser.2022.112250.